LBL-16230 c.2

# Lawrence Berkeley Laboratory

UNIVERSITY OF CALIFORNIA

RECEIVED
LAWRENCE
BERKELEY LABORATORY

AUG 29 1983

LIBRARY AND
DOCUMENTS SECTION

## Materials & Molecular Research Division

Presented at the United States-Japan Workshop on
High Field Superconducting Materials for Fusion,
San Diego, CA, May 23-25, 1983

# THE INFLUENCE OF MICROSTRUCTURE ON THE PROPERTIES OF BRONZE-PROCESSED MULTIFILAMENTARY WIRE

I.W. Wu, D.R. Dietderich, W.V. Hassenzahl,
and J.W. Morris, Jr.

May 1983

TWO-WEEK LOAN COPY

This is a Library Circulating Copy
which may be borrowed for two weeks.
For a personal retention copy, call
Tech. Info. Division, Ext. 6782.

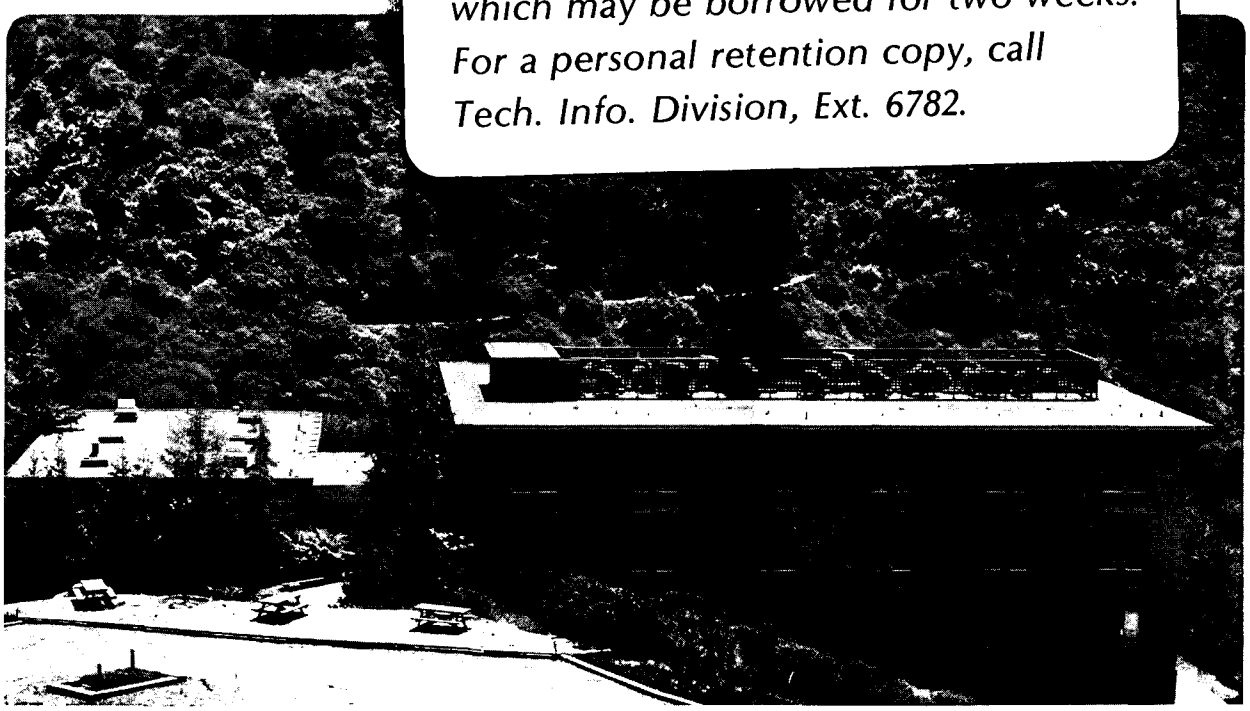

LBL-16230 c.2

Prepared for the U.S. Department of Energy under Contract DE-AC03-76SF00098

## DISCLAIMER

This document was prepared as an account of work sponsored by the United States Government. While this document is believed to contain correct information, neither the United States Government nor any agency thereof, nor the Regents of the University of California, nor any of their employees, makes any warranty, express or implied, or assumes any legal responsibility for the accuracy, completeness, or usefulness of any information, apparatus, product, or process disclosed, or represents that its use would not infringe privately owned rights. Reference herein to any specific commercial product, process, or service by its trade name, trademark, manufacturer, or otherwise, does not necessarily constitute or imply its endorsement, recommendation, or favoring by the United States Government or any agency thereof, or the Regents of the University of California. The views and opinions of authors expressed herein do not necessarily state or reflect those of the United States Government or any agency thereof or the Regents of the University of California.

# THE INFLUENCE OF MICROSTRUCTURE ON THE PROPERTIES OF BRONZE-PROCESSED MULTIFILAMENTARY WIRE

I.W. Wu, D.R. Dietderich, W.V. Hassenzahl, and J.W. Morris, Jr.

Dept. of Materials Science and Mineral Engineering, Univ. of California, and Lawence Berkeley Laboratory, Berkeley, California 94720

## SUMMARY

The A15 layer of a commercial Airco wire containing 2869 Nb filaments was analyzed as a function of heat treatment. Its microstructure is composed of three morphologically distinct concentric shells. The central shell consists of fine equiaxed grains and has a nearly stoichiometric Sn concentration. High resolution electron microscopic analysis suggests that the fine grains are formed through the polygonization of dislocations. The homogeneous composition through the fine-grained layer is a probable consequence of the small grain size, which permits relatively rapid chemical redistributions through grain boundary diffusion. In contrast, the chemical gradient in the large-grained inner and outer shells is steep.

The microstructure is established by the reaction heat treatment, and determines the critical current. The best combination of grain size, composition, and volume of the fine-grained shell is obtained with an intermediate reaction temperature (700 to 730$^{o}$C); this temperature range also yields the best values of $J_c$. Various two-step heat treatments were studied and compared to isothermal aging. The best microstructure and, hence, the best critical current characteristic was obtained by aging the specimen at 700$^{o}$C for 4 days followed by 730$^{o}$C for 2 days.

The onset transition temperature and the transition width were measured inductively. The inductive signal is apparently determined by the properties of the smallest volume of superconducting phase that is sufficient to expel the external magnetic flux. The composition gradient within this volume is then reflected in the transition width. The critical temperature first increased (to ~18K) and then decreased with increasing reaction time.

The $J_c$ characteristic of the multifilamentary wire is compared to that found in preliminary tests on an 'internal tin' bronze-processed wire fabricated by Intermagnetics General. The internal tin wire appears to have a much better critical current density at lower field. Possible metallurgical sources of the higher current density are discussed.

## ACKNOWLEDGMENT

This research was supported by the Director, Office of Energy Research, and by the Director, Office of Basic Energy Science, Materials Science Division, and by the Director, Office of High Energy Physics, US Department of Energy under contract number DE-AC03-76SF00098.

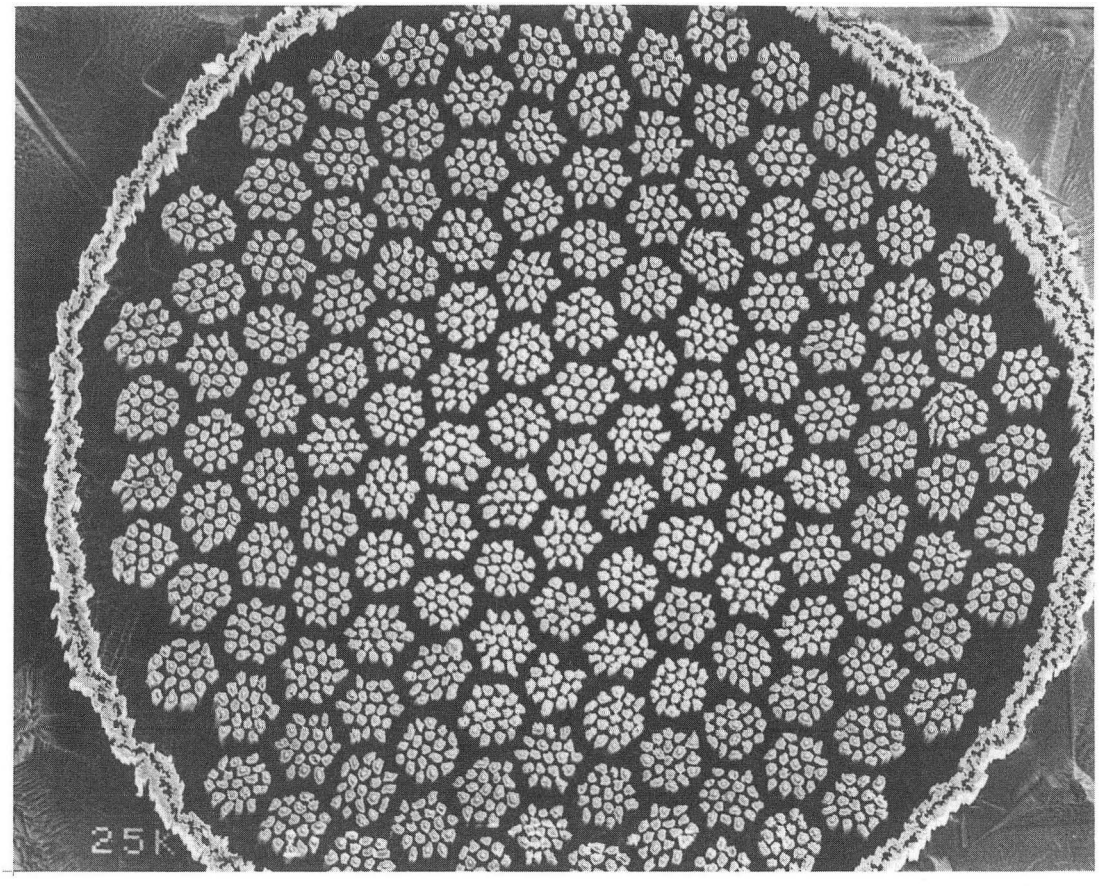


Figure 1. A scanning electron micrograph of a typical reacted bronze-processed multifilamentary wire. Notice that the Ta diffusion barrier constrains the volume expansion of the active core during the diffusion reaction, hence, the $Nb_3Sn$ diffusion layer experiences a radial compressive strain. Without this restrictive layer, the bronze matrix would be able to expand freely and not exert as much stress on the $Nb_3Sn$ layer.

XBB 831-544

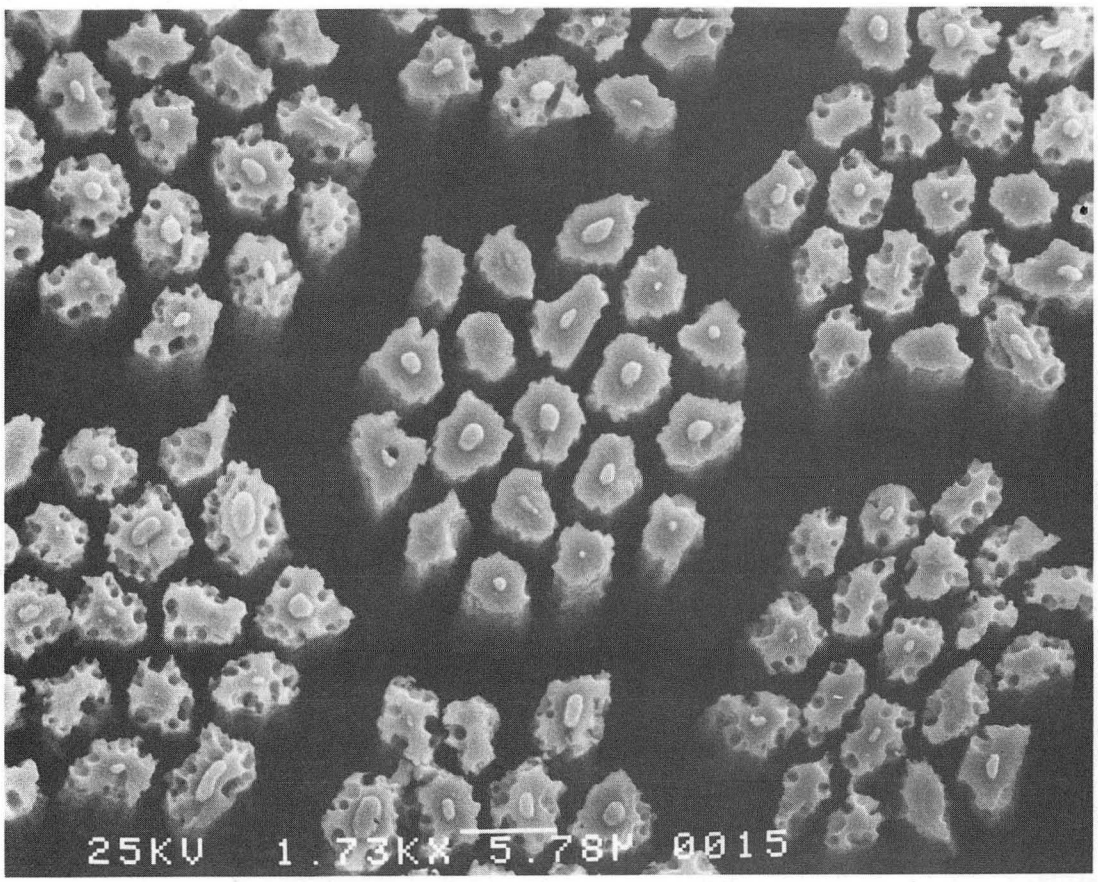


Figure 2. A scanning electron micrograph showing the $Nb_3Sn$ layer and the residual Nb filaments after the bronze matrix has been removed. Voids in the A15 layers, predominately at the periphery of the filaments, are believed to arise from the preferential etching of the A15 grain boundaries due to their high copper concentration.

XBB 831-545

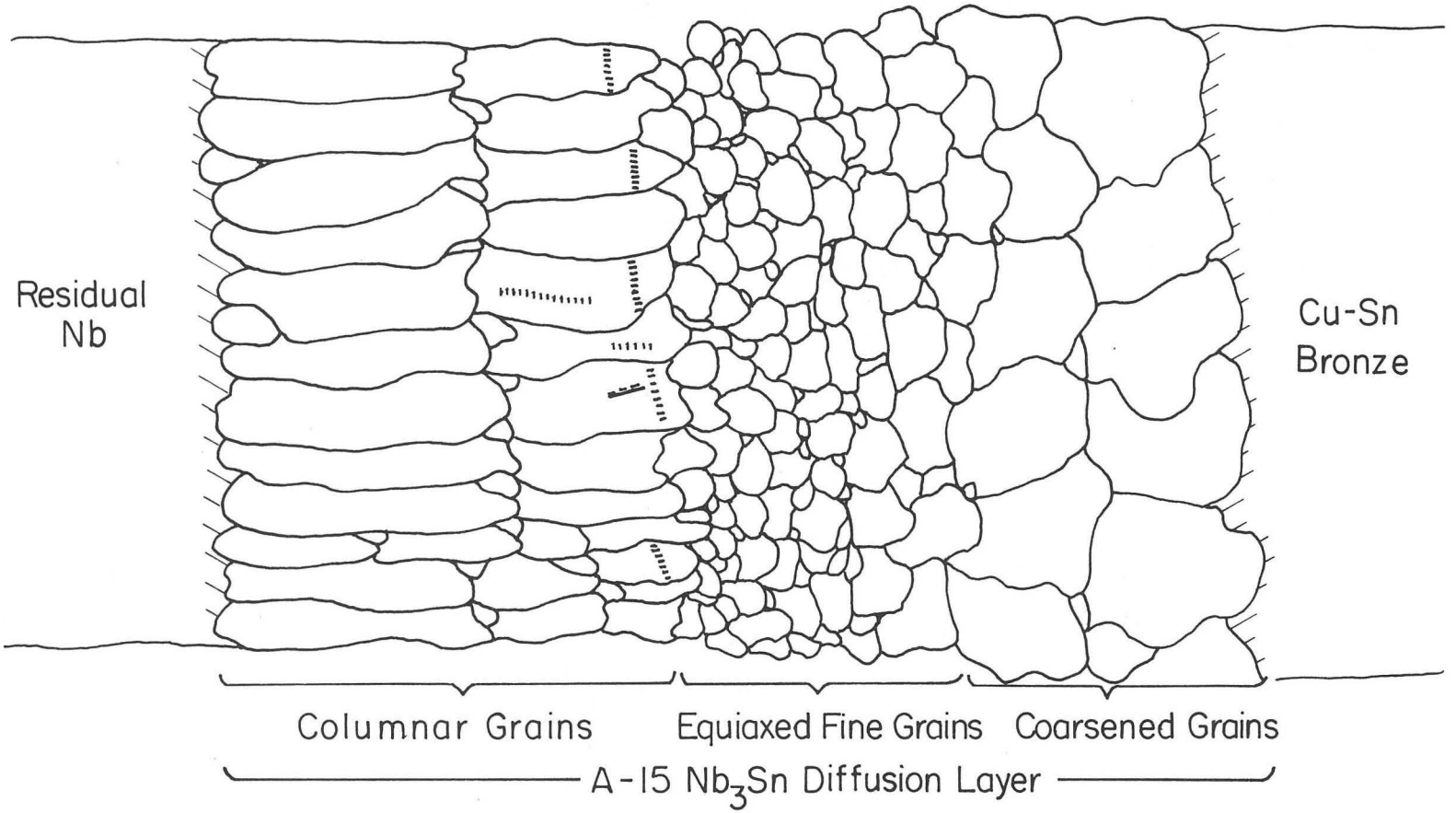


Figure 3. Schematic representation of the grain morphology of the A15 diffusion layer. The direction of the reaction is inward to the Nb filament. As a consequence, a successive layer formation followed the order: columnar grains, fine equiaxed grains and coarsened grains. The transformation of columnar grains to the fine grains is due to the polygonization of dislocation walls to reduce the strain energy associated with the $Nb_3Sn$ layer formation.

XBL 824-5549

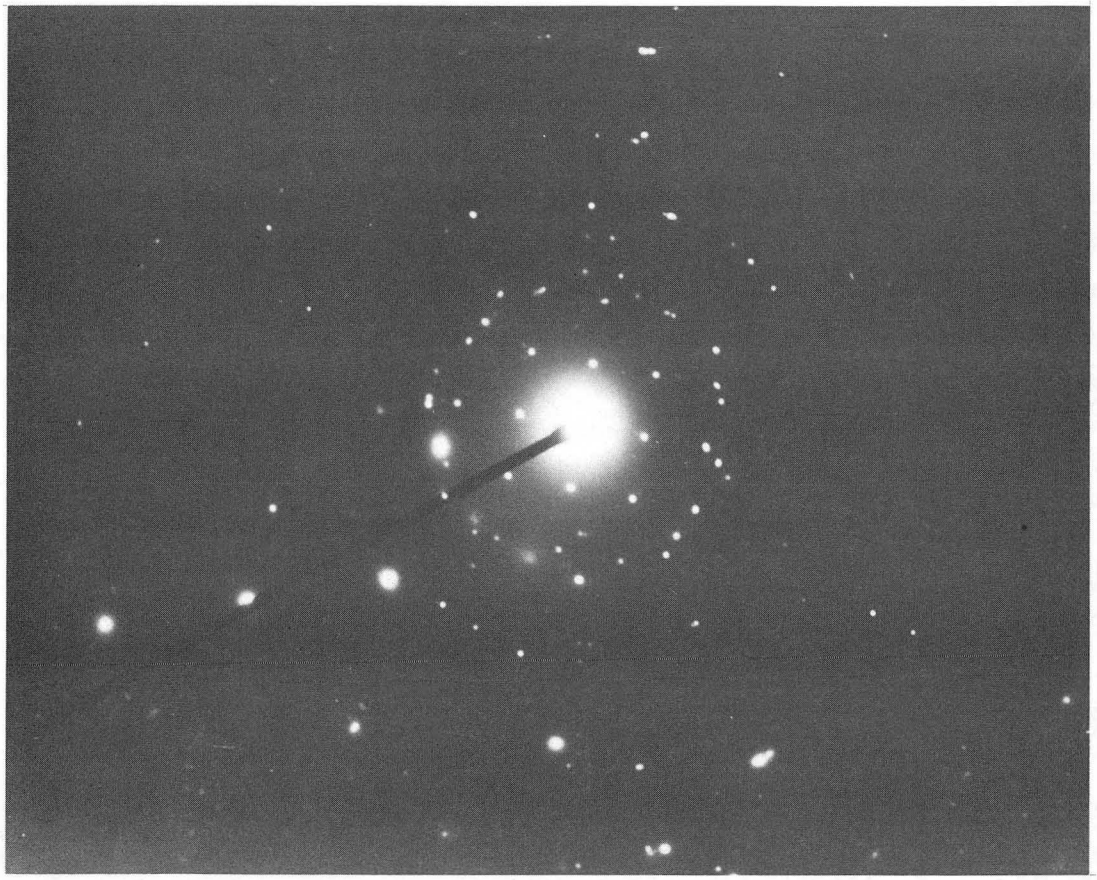

Figure 4. The selected area electron diffraction pattern of the boundary region between the A15 and the residual Nb. The square pattern near the center maximum is the (001) A15 zone axis pattern and the BCC (111) is represented by the brightest diffraction spots.

XBB 822-1159

Figure 5. The corresponding bright field micrograph of Fig. 4 showing the columnar nature of the A15 grains near the Nb interface.

XBB 818-7140

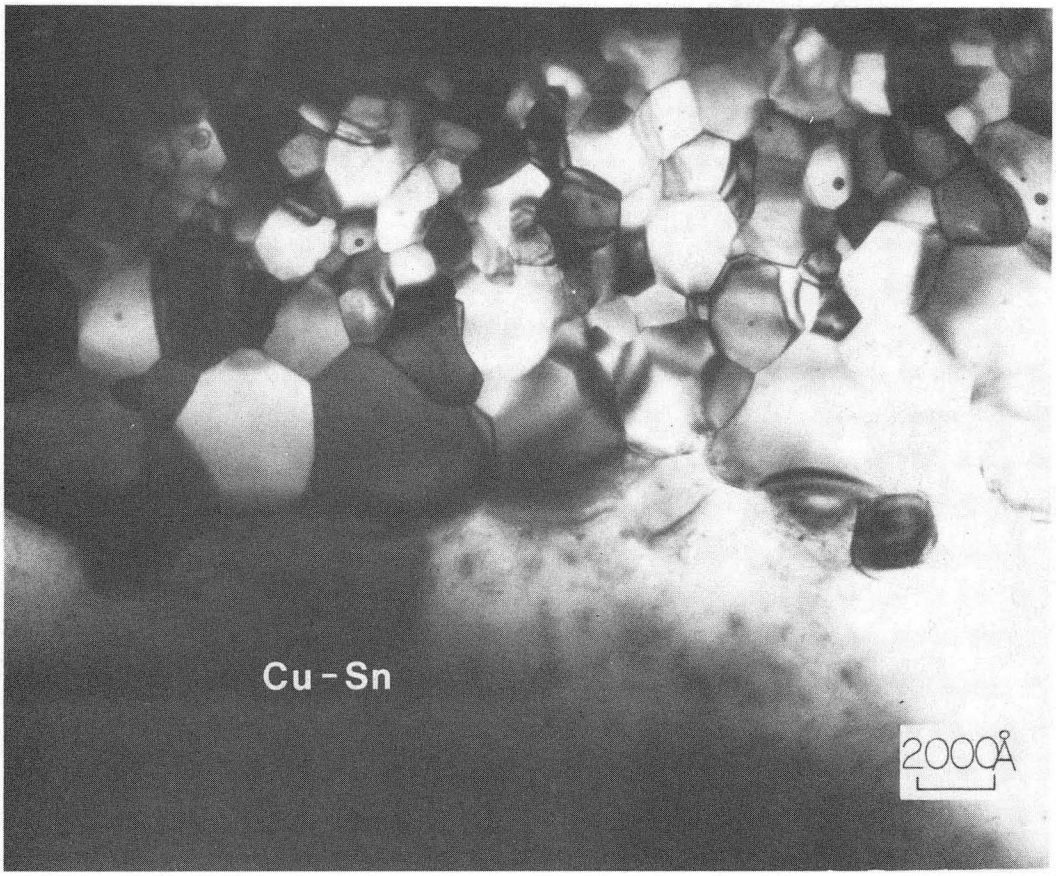


Figure 6. A TEM micrograph showing a typical $Nb_3Sn$ grain morphology near the $Nb_3Sn$- bronze interface. The coarsened large-grain layer can be seen at the periphery of the reacted filament with the fine equiaxed grain layer adjacent to it.

XBB 824-4088

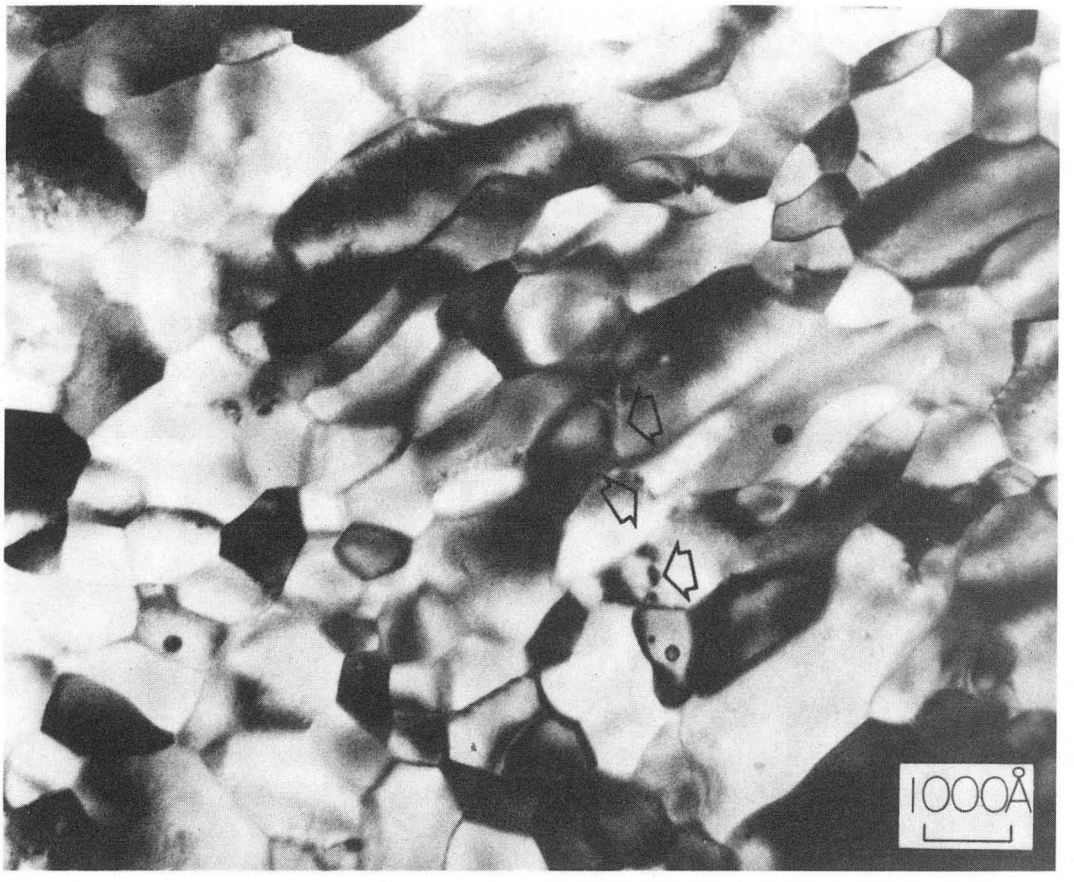


Figure 7. A TEM micrograph revealing the nature of the low angle boundaries between fine equiaxed grains along the direction of elongation of the columnar grains. The columnar grains are to the upper right of the micrograph. Several low-angle grain boundaries are indicated by arrows.

XBB 824-4087

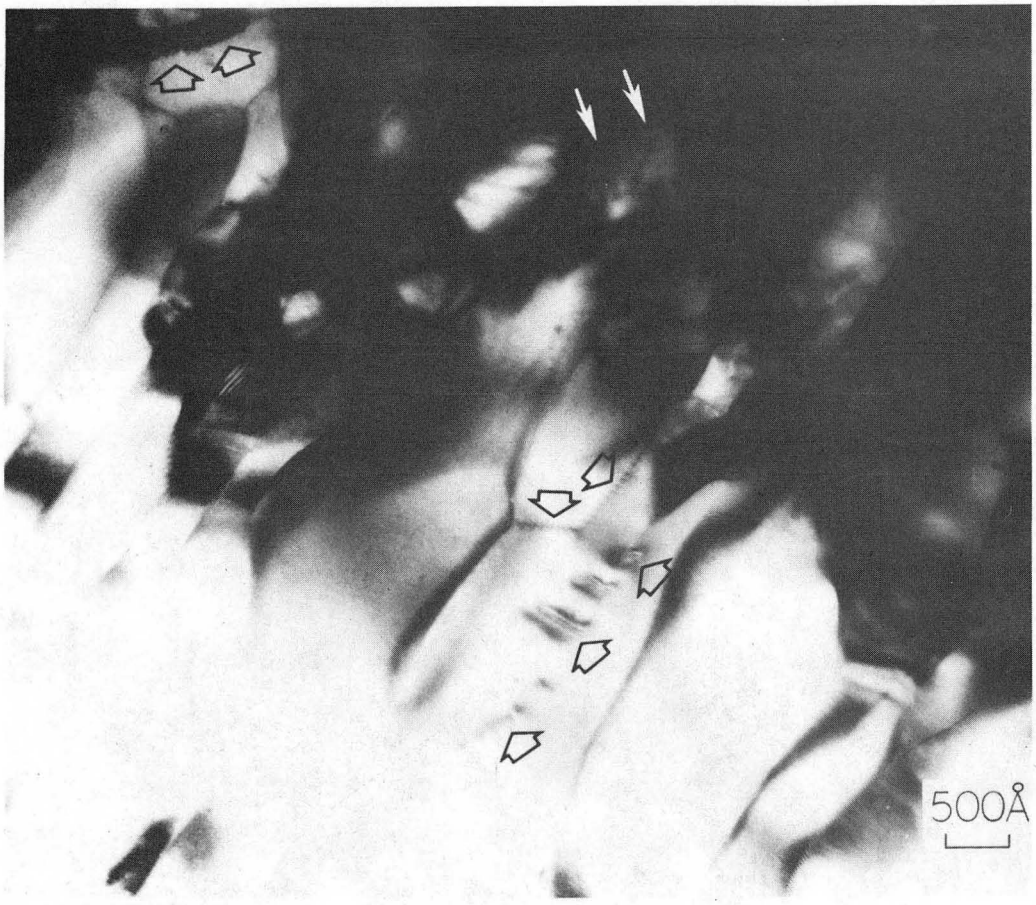


Figure 8. A high resolution TEM micrograph showing dislocation walls in the columnar grains near the Nb interface. Several distinctive dislocation walls are indicated by arrows. The driving force of the dislocations' multiplication and polygonization is believed to be the reduction of the transformation strain energy.

XBB 824-4086

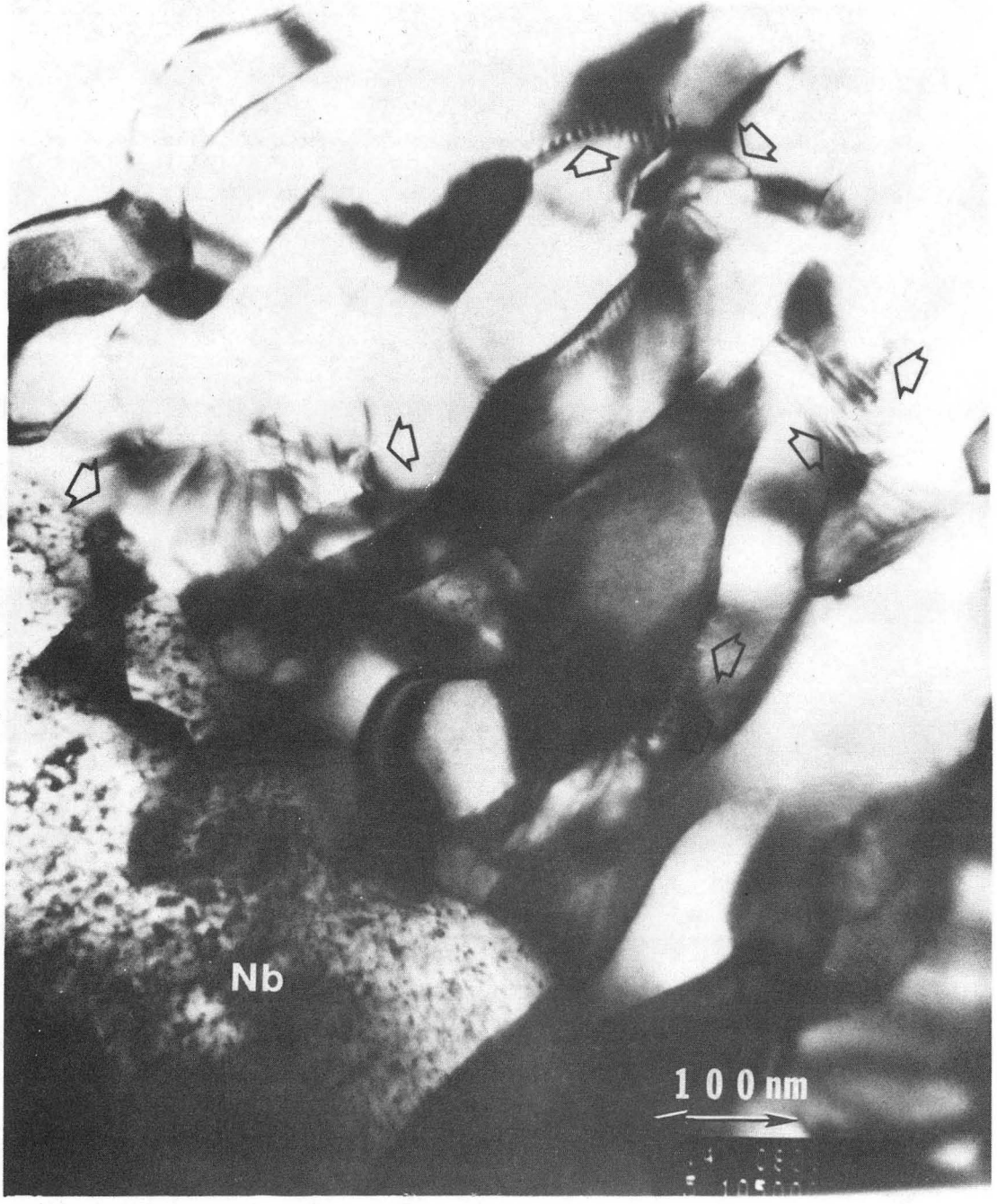


Figure 9. Another high resolution TEM micrograph showing the dislocation walls in the columnar grains near the Nb interface. Notice in the upper right corner of the micrograph that some dislocations polygonized into subgrains while some others are still in the process of polygonization.

XBB 825-4151

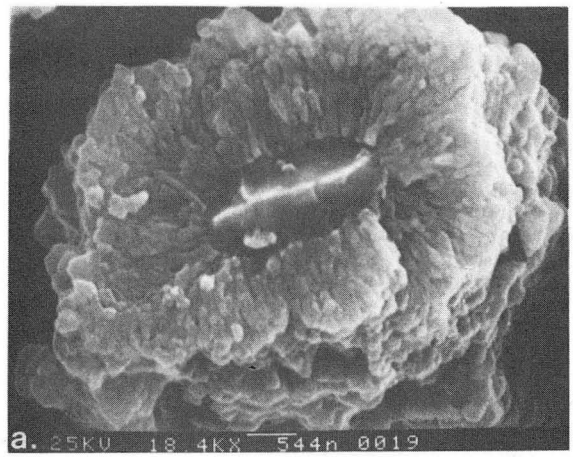


650°C/16D

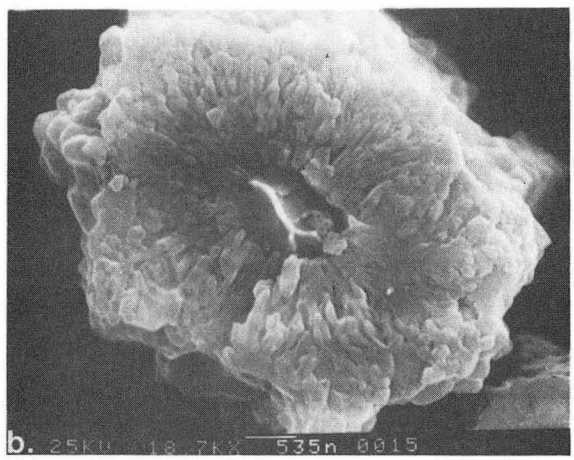


700°C/6D

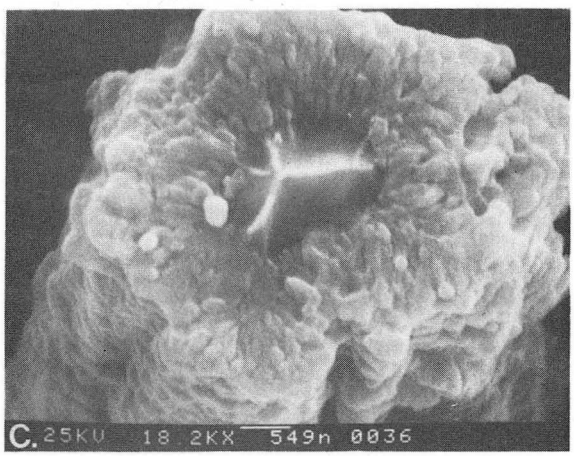


730°C/2D

Figure 10. Scanning electron micrographs of the fracture surface of individual filaments heat treated to near 90% reaction at different temperatures. The apparent grain boundaries can be distinguished by the predominate intergranular fracture mode. Lower temperature aging produces a finer grain size. However, the equiaxed grain boundaries are not revealed on the fracture surface due to the nature of the low-angle boundaries. Therefore, to accurately determine the grain size, transmission electron microscopy is required.

XBB 831-229A

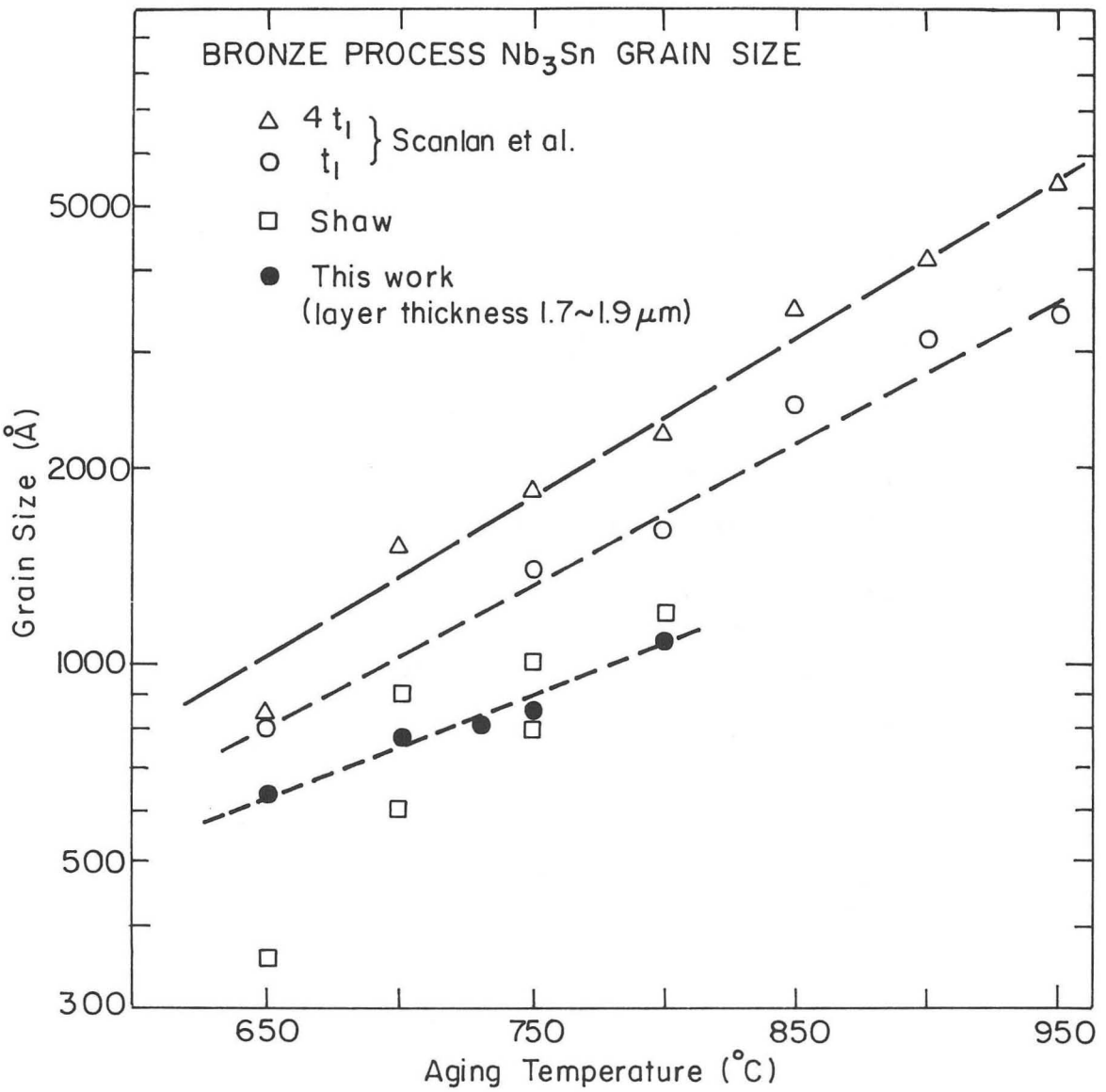


XBL 824-5611

Figure 11. The results of grain size versus aging temperature (650° to 800°C) as determined by a TEM study. The specific data shown in this figure are from the samples heat treated up to the time required to yield a layer thickness ranging from 1.7 to 1.9 ;m. Two other data in the literature on grain size are also included for comparison. It can be concluded that the grain size increases with increasing aging temperature and time, and decreases with decreasing filament diameters.

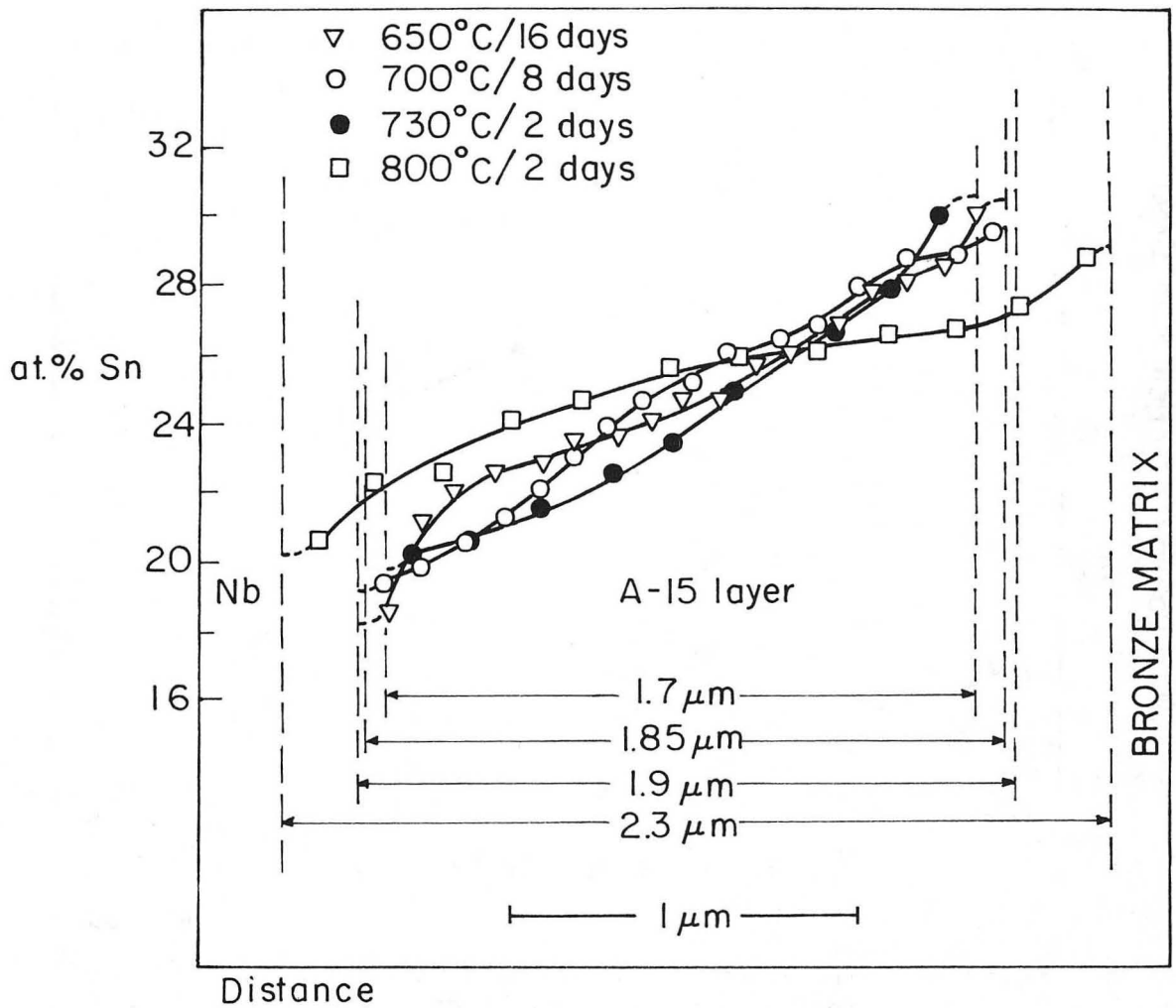


XBL 831-5054

Figure 12. Tin concentration profiles determined by STEM/EDXS analysis across the reacted A15 layer for samples aged to near 90% reaction at various temperatures. The tin concentration decreases monotonically through the layer from a Sn-rich composition at the bronze interface to a Sn-poor composition at the Nb interface. The central region of the A15 layer, where the grain size is small and equiaxial, has a composition close to stoichiometry. The general trend is for the tin concentration gradient to decrease with increasing aging temperature and time.

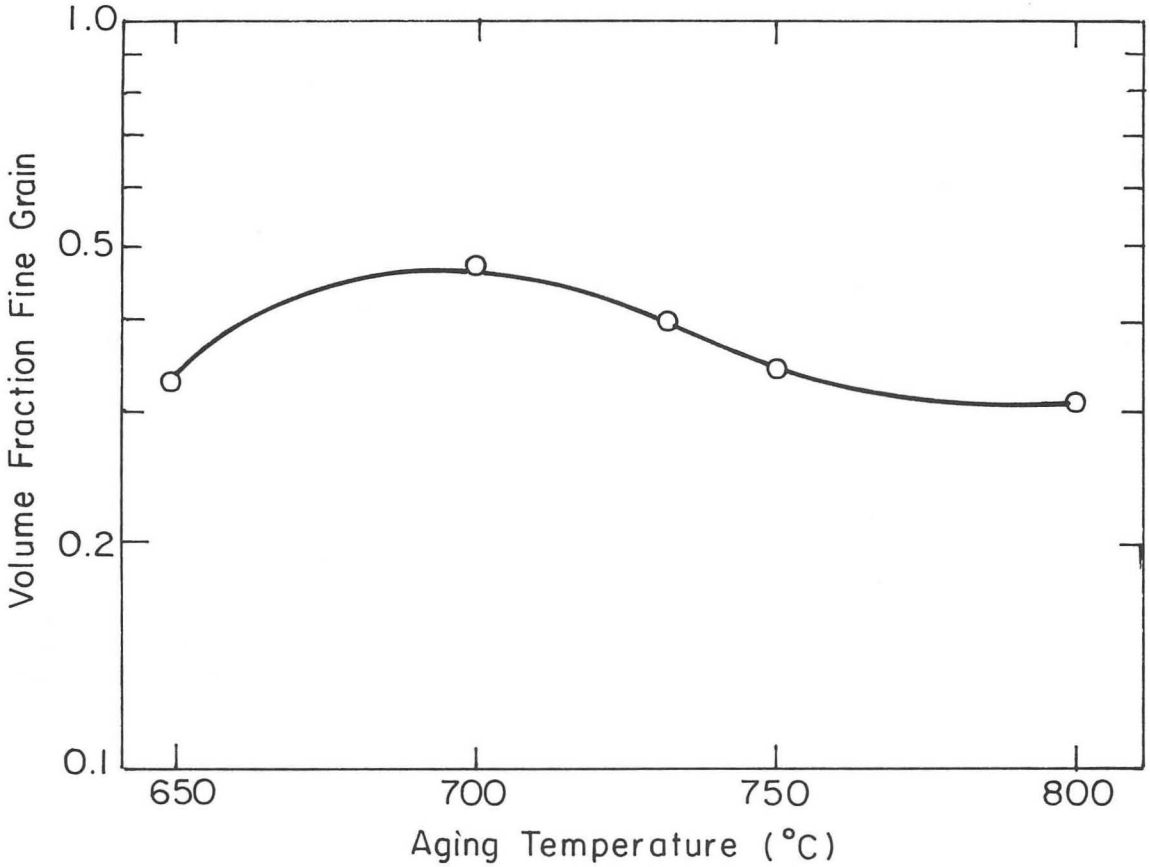


XBL 825-5641

Figure 13. The volume fraction of the fine-grain layer with respect to the original Nb volume versus aging temperature for samples near full reaction. Since this layer contains high density grain boundaries and a near stoichiometric composition, it is the volume that carries the majority of the current near $J_c$. Two competing factors determine the volume of the fine-grain layer: the mobility of dislocations to polygonize and grain coarsening. Therefore, an optimum temperature (from 700 to 730°C) produces the maximum fine-grain volume.

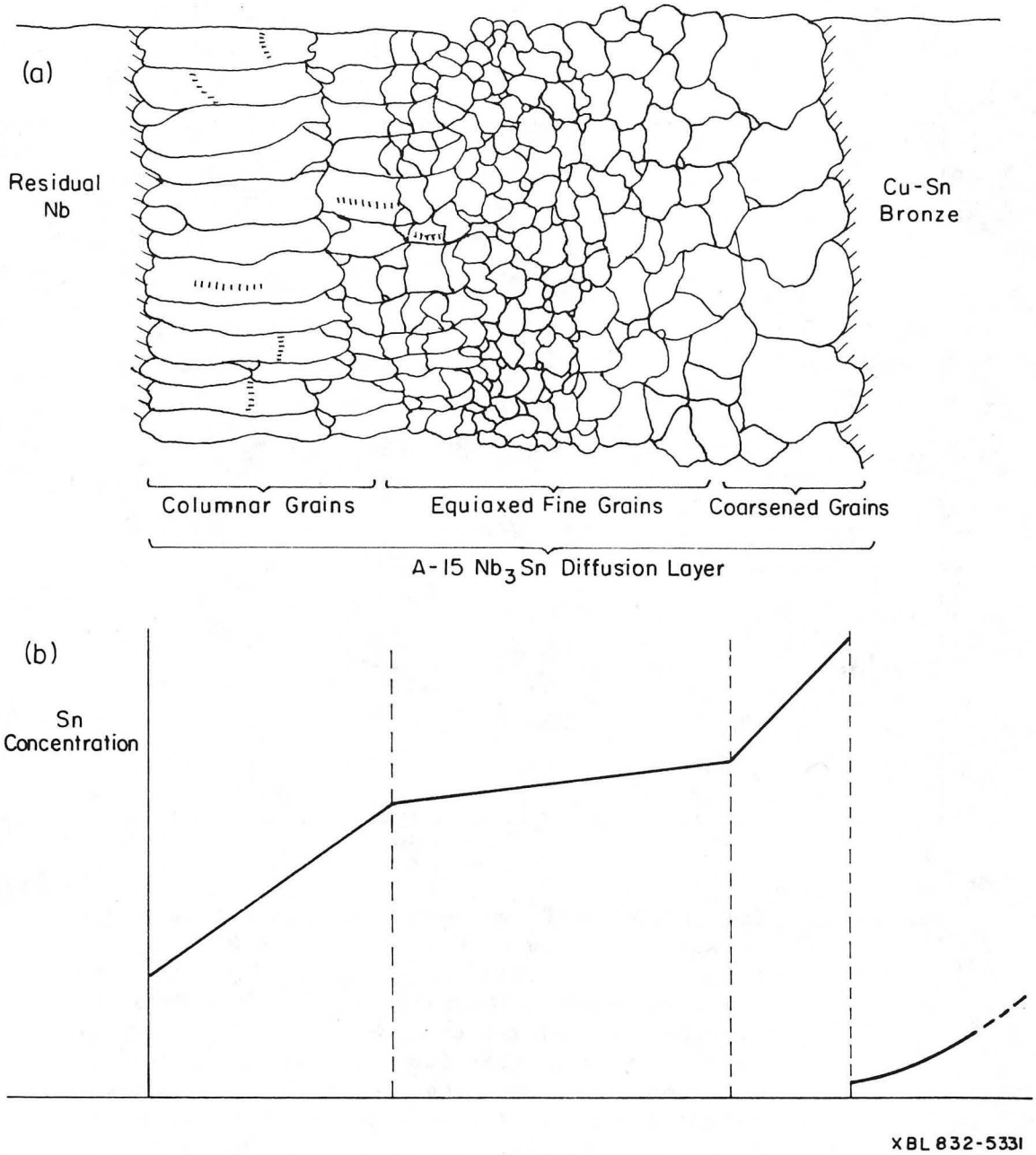


Figure 14. A schematic representation of (a) the grain structure and (b) the tin concentration profile across the A15 layer. It is believed that the flat concentration profile in the fine-grain layer is due to the fast distribution of tin along the grain boundaries.

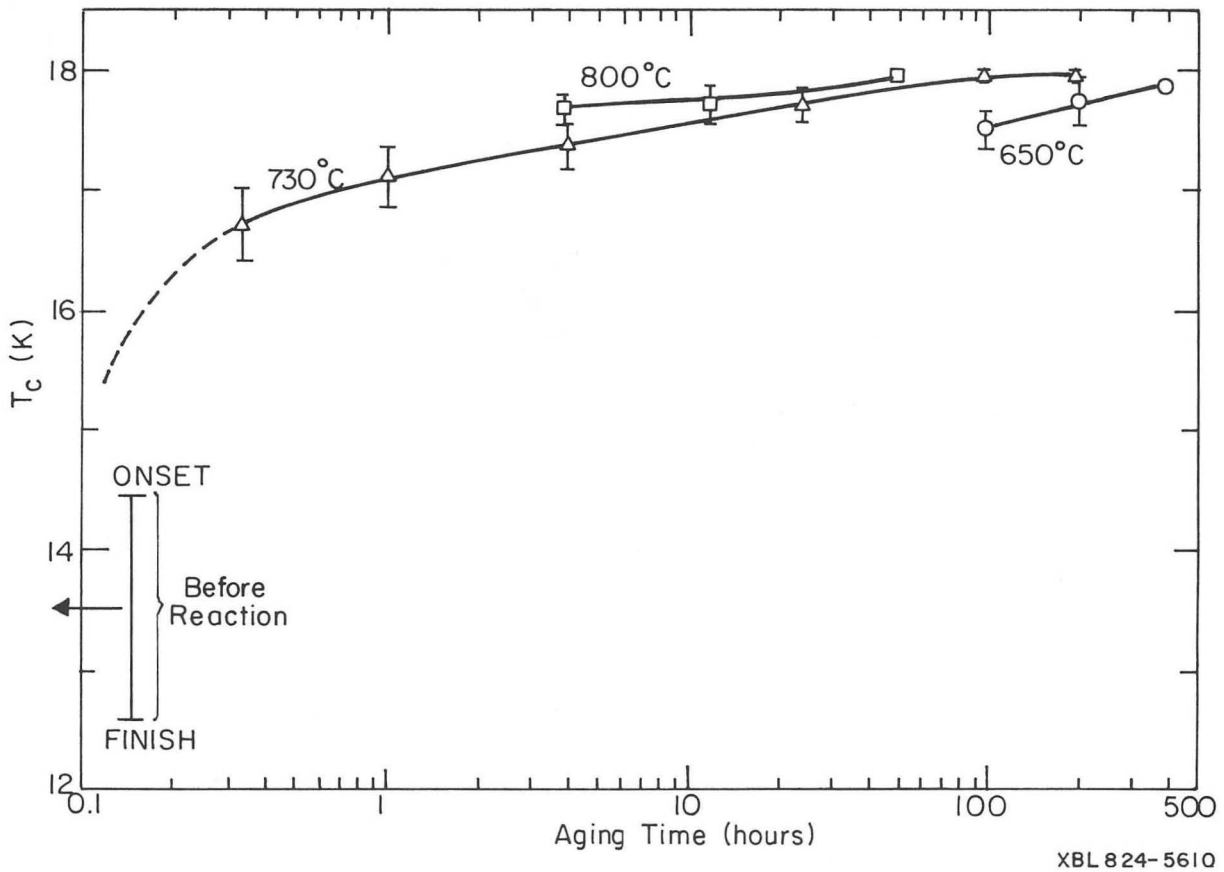


**Figure 15.** The inductive $T_c$ midpoint and transition width versus aging time for 650, 730 and 800°C. The $T_c$ midpoint increases (to near 18K) and its width decreases with aging time. This behavior is quite general for bronze-processed wires. It can be concluded that the inductive measurement, which measures the change in slope of M-H curve within the field range of the applied oscillating field amplitude, yields only the information about the volume of superconducting phase enough to expel the external flux. In our measurement, this volume is estimated to be ~1 μm in layer thickness.

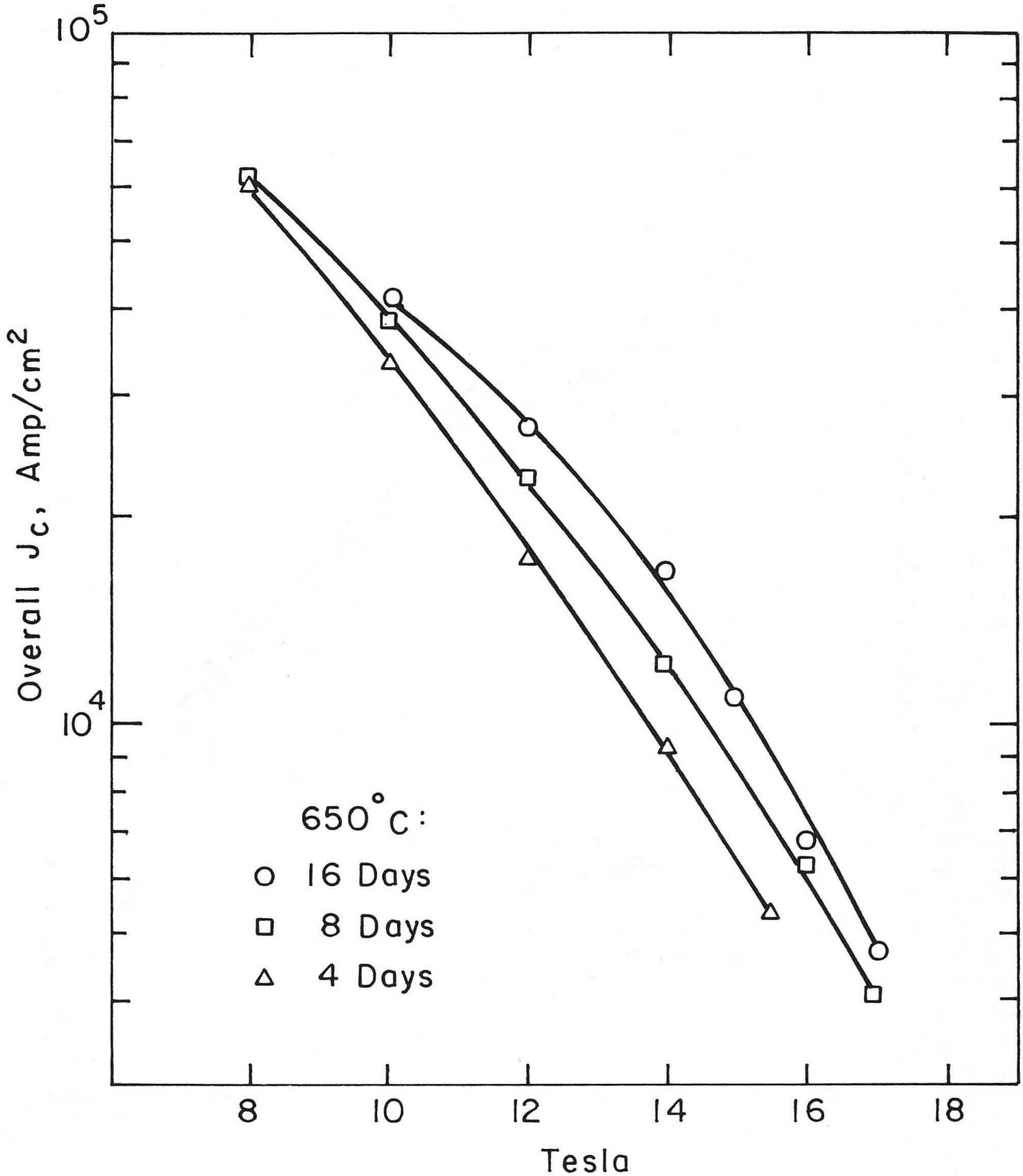


XBL 822-5156

Figure 16. The $J_c(H)$ characteristics of samples aged at 650°C. Microstructural studies revealed that the fine grain size for short heat treatments are responsible for the high $J_c$ at lower fields even though the volume of the fine grain layer is smaller and has a higher concentration gradient. Prolonging the aging time to 16 days mainly increases $J_c$ at higher fields.

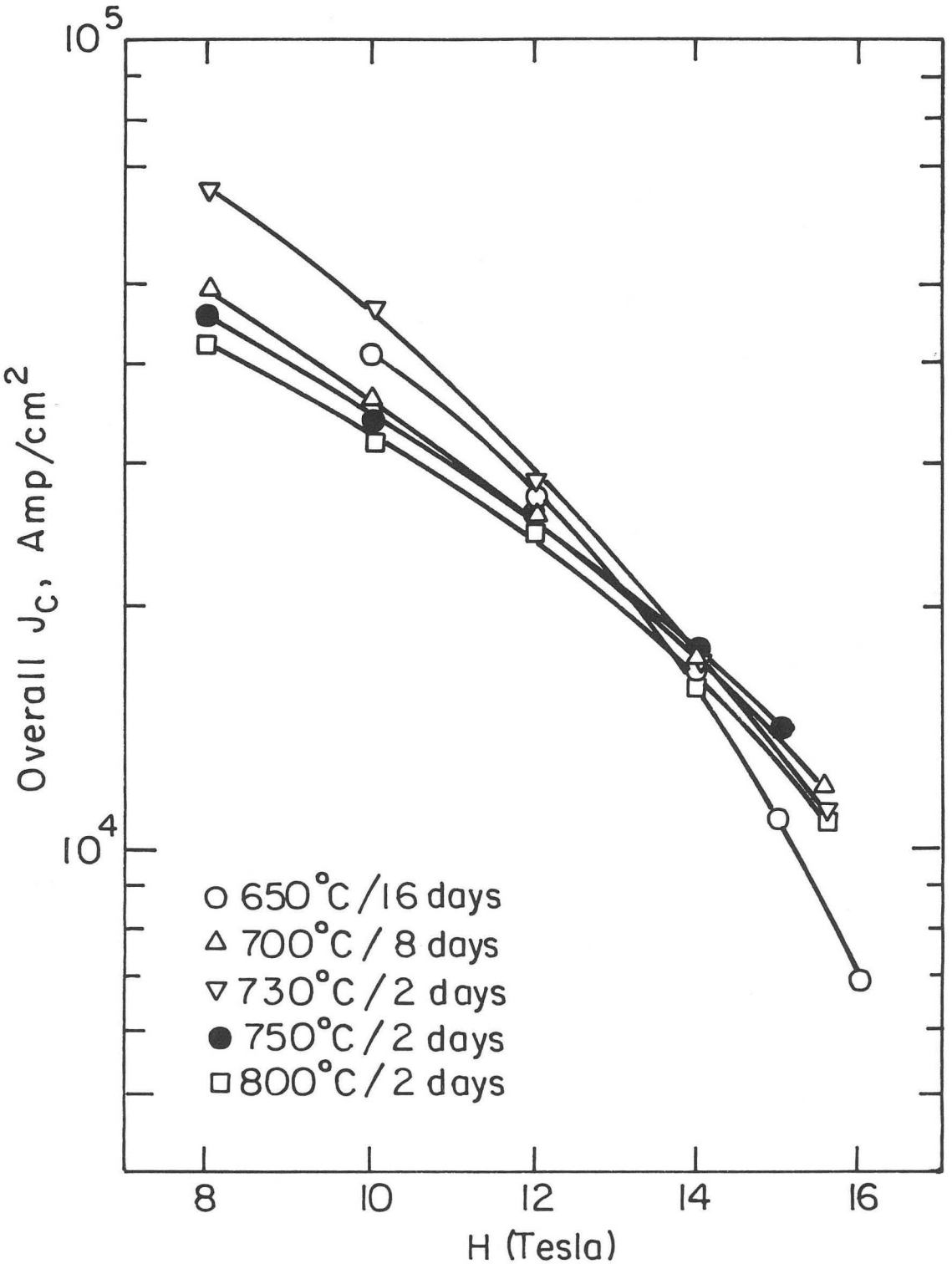


XBL 831-5059

Figure 17. The $J_c(H)$ characteristics of samples heat treated in the temperature range 700 to 800 °C. Heat treatments at intermediate temperature and time give the best $J_c(H)$ characteristics. For example, samples aged at 700°C for 6 days and 730°C for 2 days show the best $J_c$ at all fields.

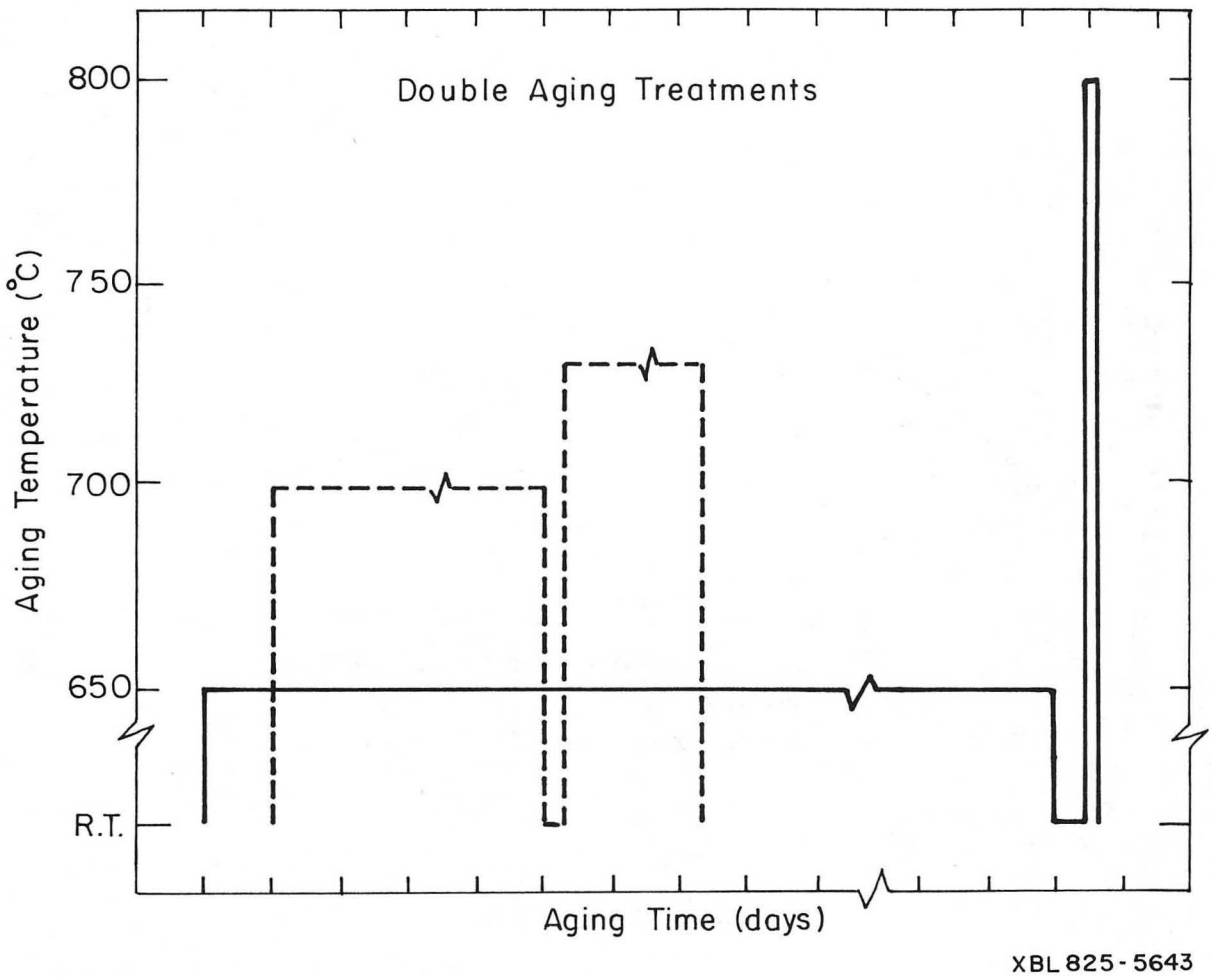


Figure 18. Schematic heat treatment schedules to improve the microstructural state of A15 layers. The first-stage heat treatment is at a low temperature to establish a fine-grain structure and the second-stage heat treatment at higher temperature is designed to redistribute the tin within the fine-grained layer. The necessary condition for this modified heat treatment to work is that the redistribution of tin be a faster process than the $Nb_3Sn$ grain coarsening introduced by the second-stage higher temperature treatment.

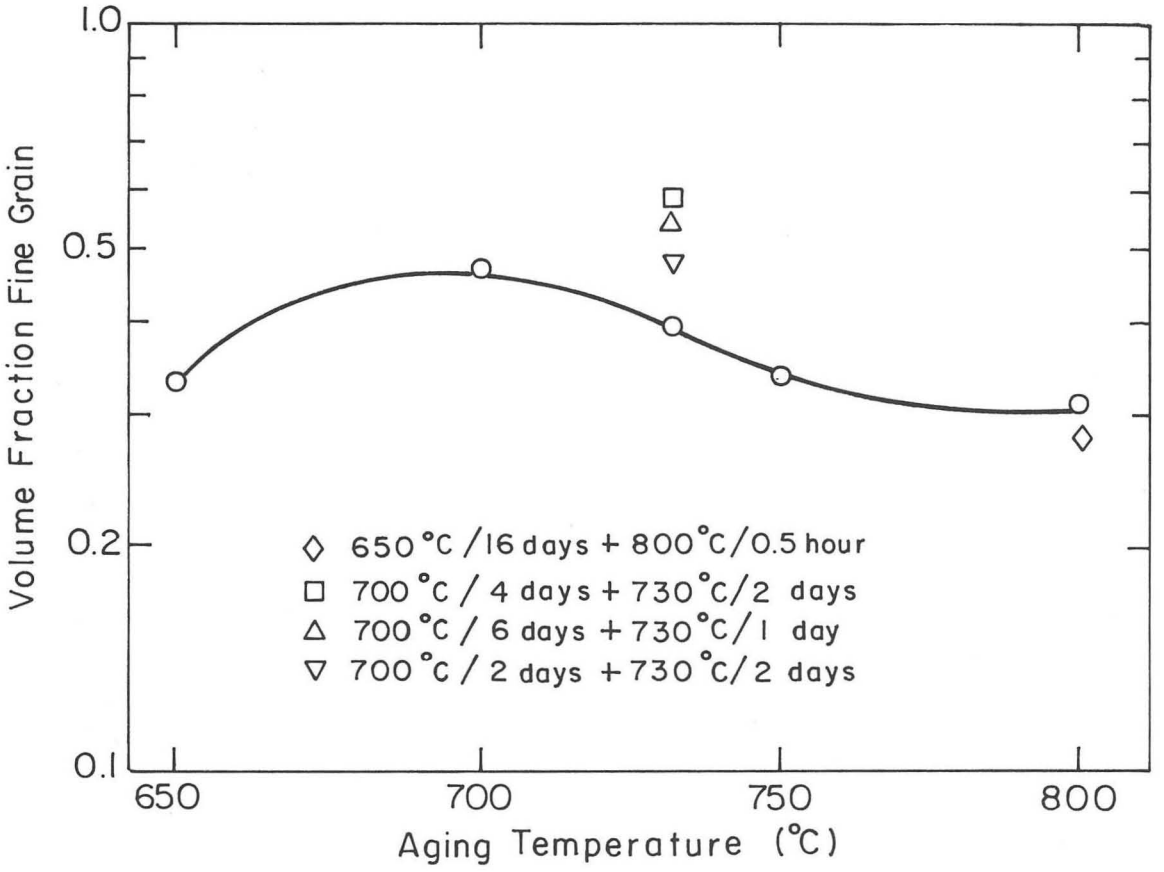


XBL 825-5642

Figure 19. The volume fraction of the fine grain layer for several double-aged specimens as compared with that of the isothermally prepared samples. The samples aged at 700°C and then followed by 730°C show an increase in the volume fraction, while the 650°C + 800°C heat treatment produces a lower fraction. This can be attributed to the increase in the dislocation mobility without significant coarsening at the 730°C treatment.

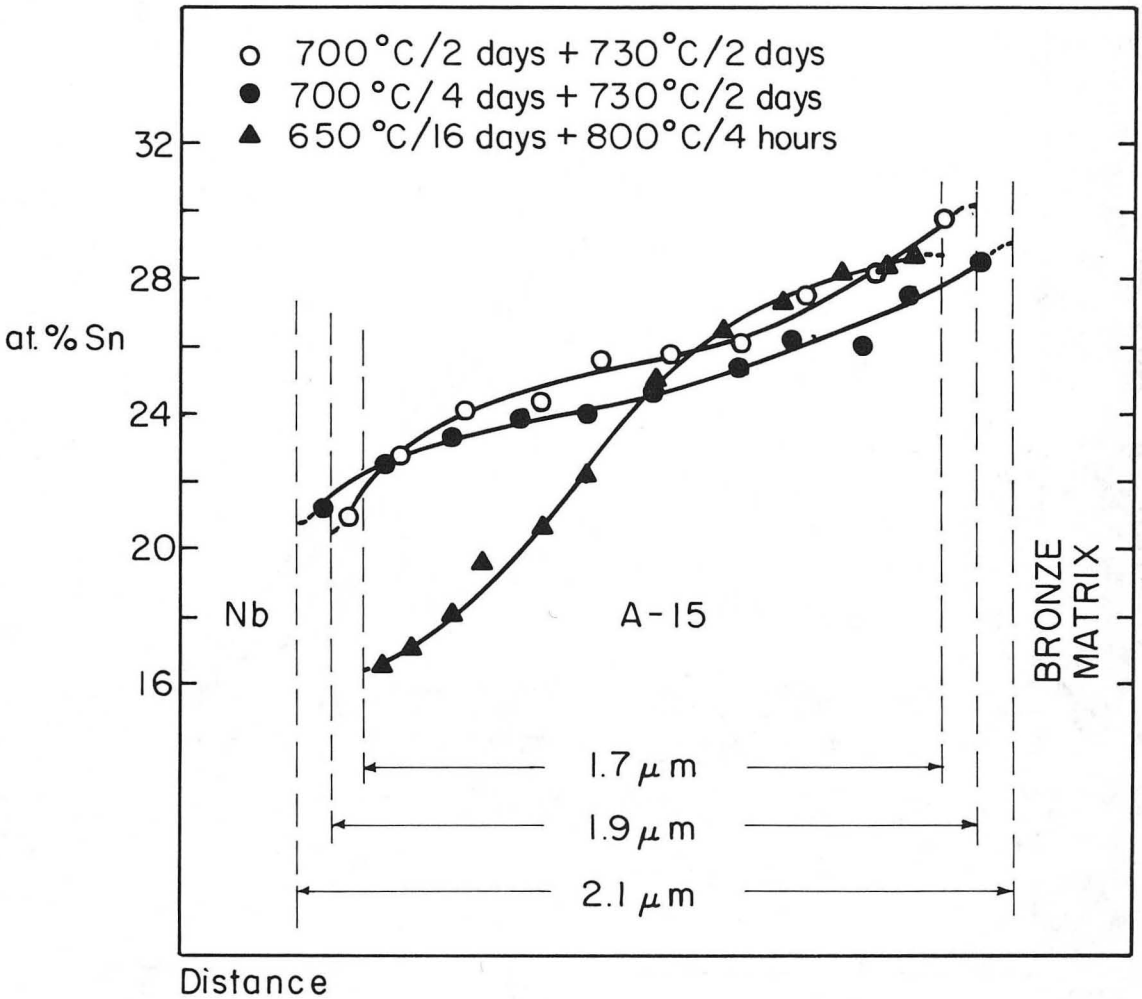


XBL 817-6193

Figure 20. The STEM/EDXS analysis of the tin concentration profiles of three double-aged specimens. The small composition gradient of the 700 + 730°C aged specimens shown in this figure is favorable, while the steep gradient of the sample treated at 650°C for 16 days + 800°C for 4 hours is undesirable and yields inferior $J_c$.

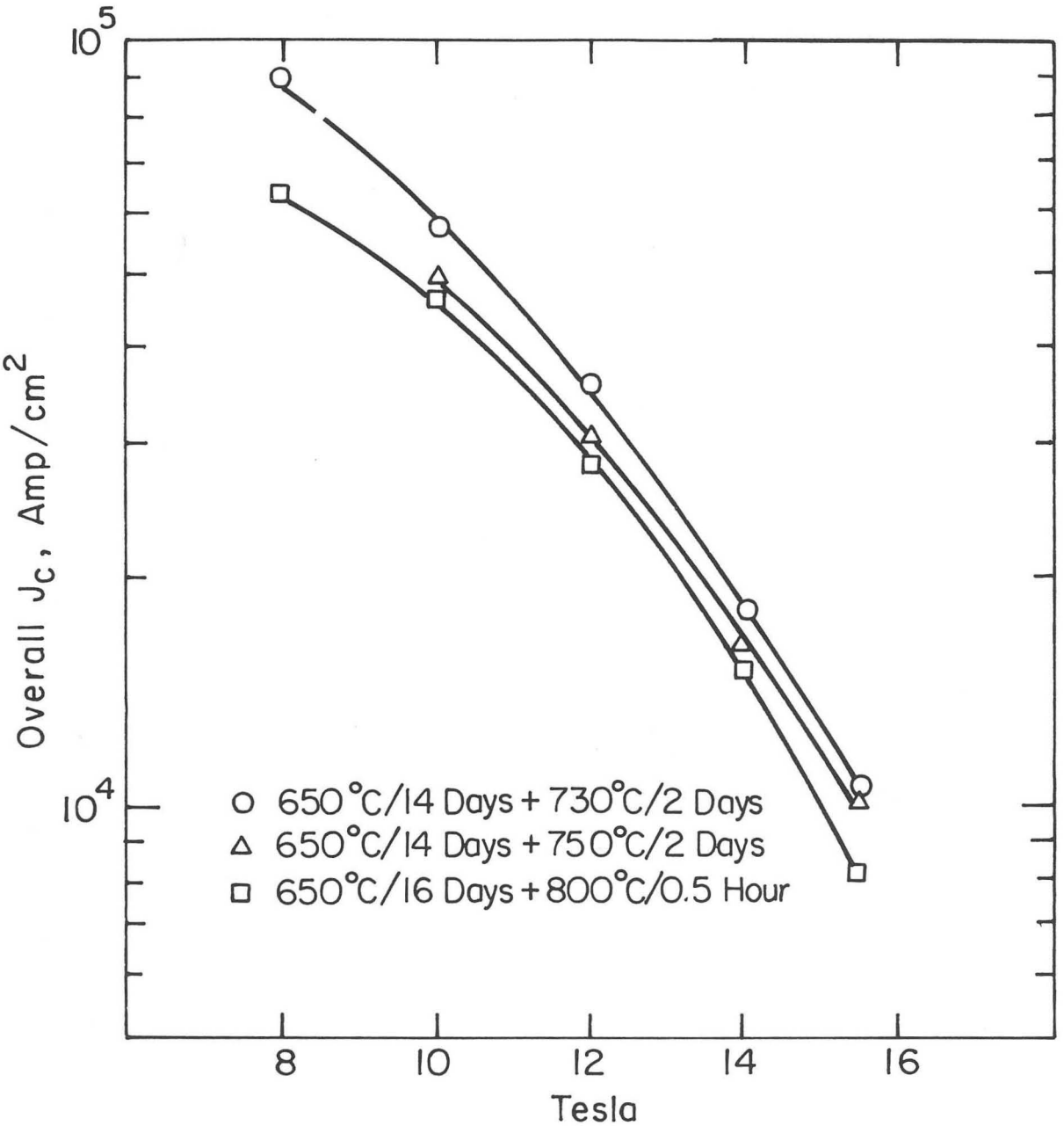


XBL 822-5158

Figure 21. The $J_c(H)$ characteristics of double-aged specimens starting with 650°C and followed by various higher temperature treatments. From the data it is clear that the higher the second aging temperature, the smaller the $J_c$ enhancement.

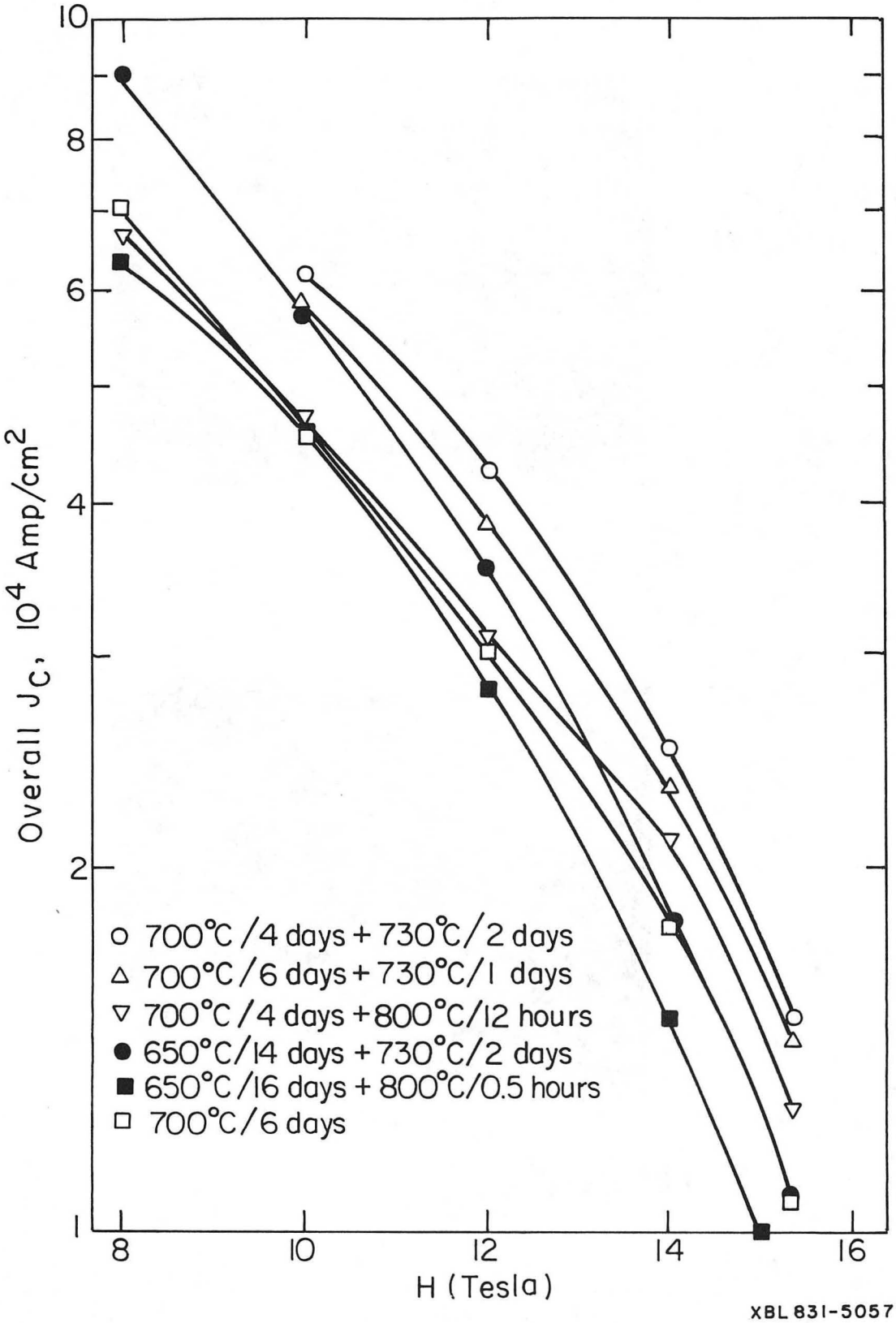


Figure 22. The $J_c(H)$ characteristics of several double-aged samples with 700°C as the starting heat treatment temperature. The $J_c(H)$ of the 700°C/6 days sample is also included, representing the best obtained by isothermal aging. The 700°C/4 days + 730°C/2 days sample has about a 50% increase in the $J_c$ over that of the 700°C/6 days.

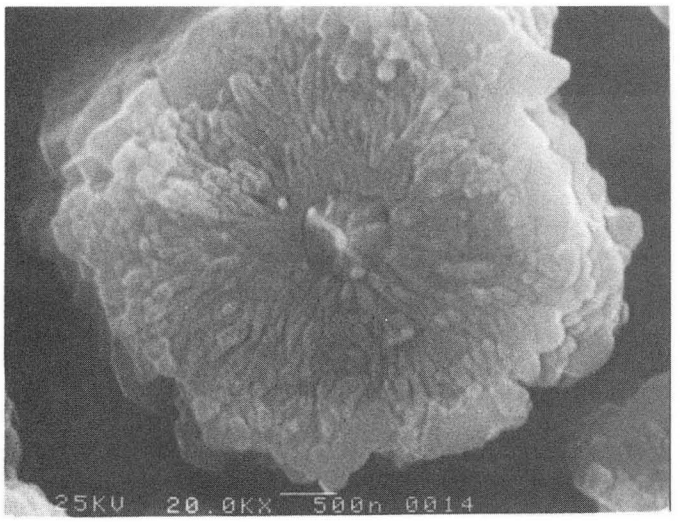


(a) 650°C/14D, 730°C/2D

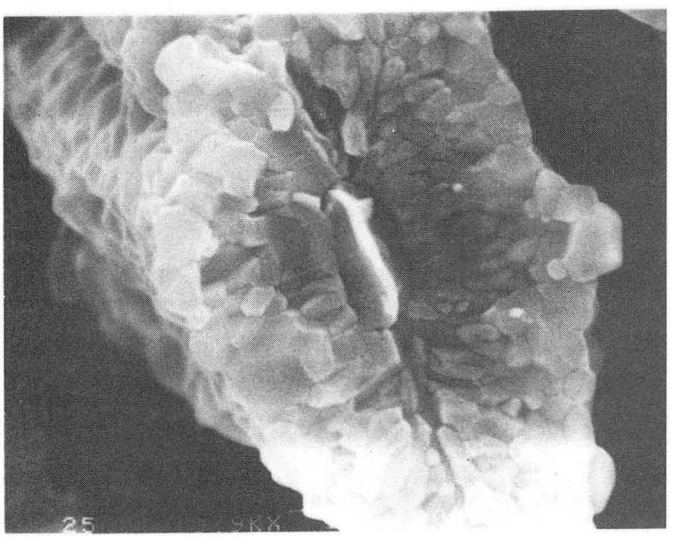

(b) 800°C/2D

Figure 23. The SEM micrographs of the fracture filaments aged at (a) 650°C/14 days + 730°C/2 days, and (b) 800°C/2 days. A significant difference in the apparent grain size with varying heat treatment conditions can be noticed. Also, the intergranular fracture mode of the A15 phase is very distinct (b).

XBB 824-4084

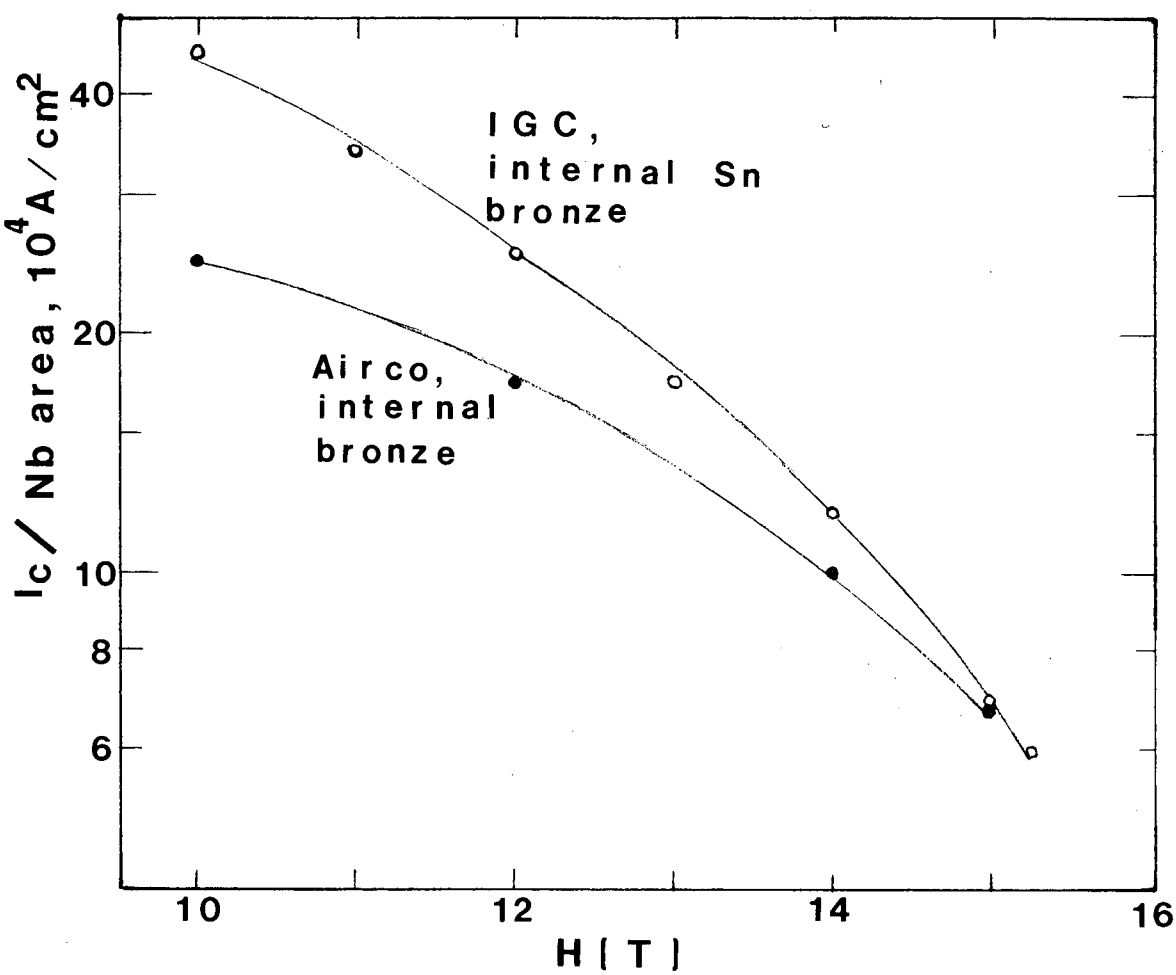


XBL 836-10200

Figure 24. A comparison of $I_c(H)$ divided by the initial Nb area of the 'internal bronze' Airco wire and the 'internal tin bronze' IGC wire. The Airco wire data in this figure is the best obtained by double-aging treatment. The IGC sample cited in this figure represents the best heat treatment condition of a recent preliminary study. By optimizing the heat treatment, it is expected that this value can be improved further. A significant increase in $J_c$, especially in the lower field range, is clear. The improvement is most likely due to the microstructural sources introduced by the change of diffusion condition.

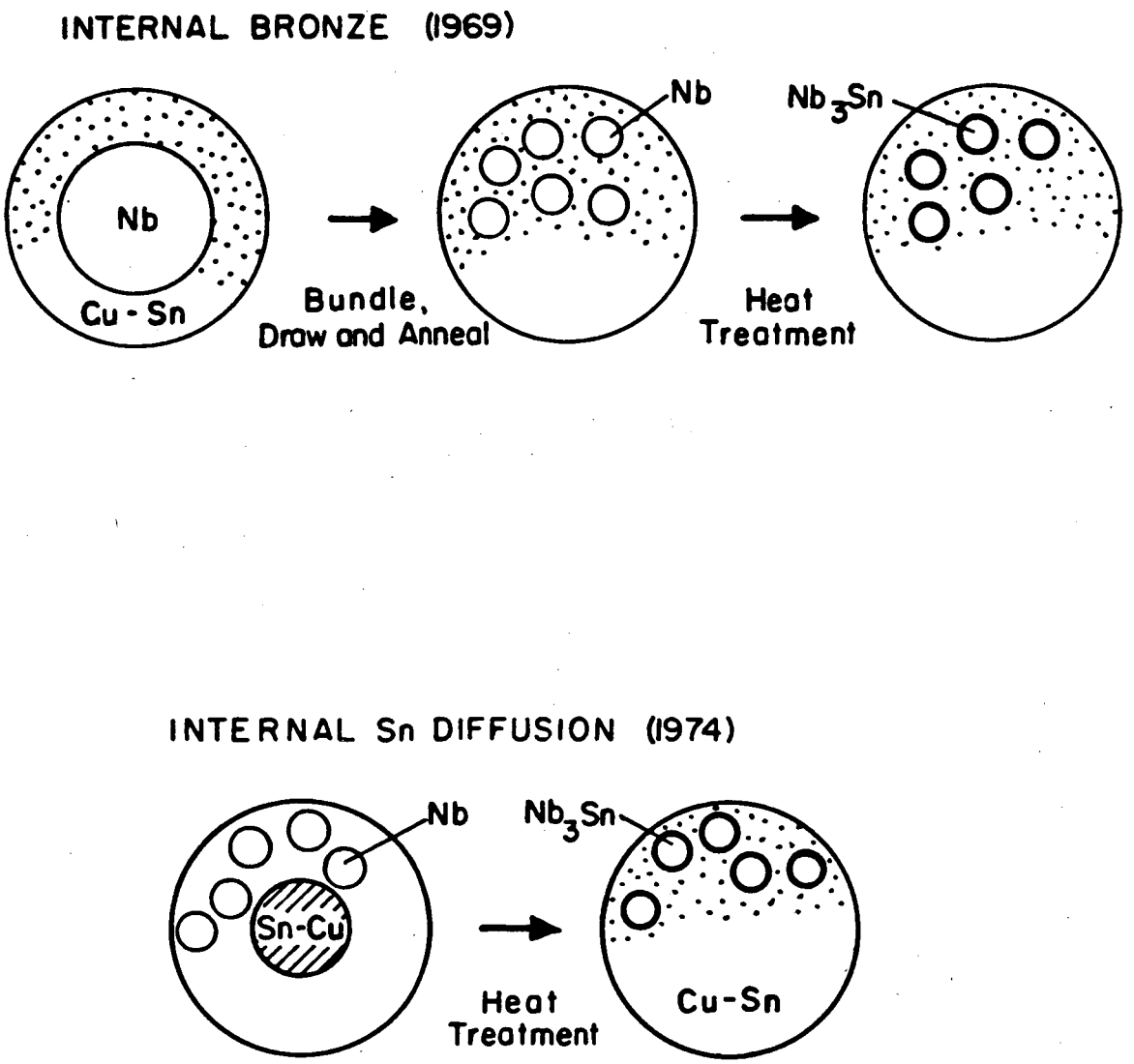


XBL 836-10199

Figure 25. Schematic rep resentations of the 'internal bronze' and the 'internal tin bronze' processes for the multifilamentary $Nb_3Sn$ wire. It can be recognized that the main difference between these two processes is that the 'internal tin bronze' process has a continuous supply of tin instead of sequential depletion of tin in the bronze matrix. The grain size will be smaller due to a higher nucleation rate. The fact that it is easier to draw the wire down to smaller size encourages finer filaments. The fine filaments will, react thus eliminating the low tin con centration boundary at the Nb interface. As a result, a larger volume of the A15 phase can be closer to stoichiometric composition.

This report was done with support from the Department of Energy. Any conclusions or opinions expressed in this report represent solely those of the author(s) and not necessarily those of The Regents of the University of California, the Lawrence Berkeley Laboratory or the Department of Energy.

Reference to a company or product name does not imply approval or recommendation of the product by the University of California or the U.S. Department of Energy to the exclusion of others that may be suitable.

*TECHNICAL INFORMATION DEPARTMENT*
*LAWRENCE BERKELEY LABORATORY*
*UNIVERSITY OF CALIFORNIA*
*BERKELEY, CALIFORNIA 94720*